CHAPTER (2)

LITERATURE REVIEW AND METHODOLOGY

2.1 INTRODUCTION

Crude oil is an organic liquid substance often found below the Earth's surface. It is made up of thousands of molecules composed of different hydrogen and carbon atoms. Such compounds are called hydrocarbons. These hydrocarbons also contain different proportions of impurities like oxygen, sulphur, nitrogen and heavy metal atom. Oil is formed from the accumulation of hydrocarbons. Hydrocarbons accumulate naturally, thousands of feet below the surface of the Earth, from the decomposition of organic materials like plants and marine. Trapped beneath the ground under enormous pressure and high temperatures, these hydrocarbons were compressed and eventually transformed into crude oil after millions of years (Haderer M, 2013).

This chapter is composed of two parts; in the first part the history of using satellite images for oil exploration will be discussed where the second part is an introduction about remote sensing which includes information about electromagnetic energy, spectral signature for objects and some interpretation basics.

2.2 OIL EXPLORATION HISTORY

Exploration for hydrocarbons (oil, gas, and condensate) is commonly acknowledged to have begun with the discovery at Oil Creek, Pennsylvania, by "Colonel" Edwin Drake in 1859. However, this was only the start of the modern global era of technology-driven advances in exploration. Traditionally, oil exploration was conducted by recognizing seeps of hydrocarbons at the surface. The Chinese, for example, used oil (mostly bitumen) obtained from seeps in medication, waterproofing, and warfare several thousand years ago (Sunstar, 2008).

Even Drake's well, the first to intentionally look for oil in the subsurface, was based on direct identification of seeped hydrocarbons at the surface. In fact, most oil until the turn of the twentieth century was in one form or another related to seep identification. However, one theory developed during this time was to have a profound impact on exploration.

Aerial remote sensing for features favored for hydrocarbon accumulation became an important and effective technique, particularly in areas of sparse vegetation cover following World War II when low-cost, rapid reconnaissance of large areas became feasible. Large-scale features such as faults and folds could be identified and targeted for detailed seismic acquisition. In the 1970s, this capability was improved dramatically by the use of satellite remote sensing technologies (LANDSAT) (Sunstar, 2008).

From the 1940s to the 1960s, there were important developments in the understanding of the controls on lateral and vertical variations within reservoir sequences. In particular, the new discipline of *Sedimentology* used modern depositional analogues from around the world to understand the nature, distribution and controls over ancient reservoir sequences.

By the beginning of 1970s, there was a significant advance in the power and reduction in size and cost of computers that has lead directly to a dramatic increase in the ability of geophysicists to acquire, process, and interpret large quantities of seismic data. Initially, this was in the form of 2-D reflection seismic onshore, but this trend has continued to the present day and now oil companies regularly undertake, mostly offshore, 3-D seismic surveys. Three-dimensional surveys are repeated over the same area every few years to monitor fluid movement within reservoirs and thereby optimally manage hydrocarbon recovery. Highly complex three-dimensional models of the subsurface can be displayed on sophisticated workstations or in the form of a fully enclosed room where staff can be totally immersed in the data using special glasses and can "walk through" the reservoirs to, for example, choose the optimal location and direction of wells (Sunstar, 2008).

2.2.1 History of Oil Exploration Using Satellite Images

Remote sensing techniques have been employed by numerous researchers in investigating numerous geologic problems, with varied results (Sikabonyi et al, 1959). The use of remotely sensed data has been suggested for mapping rapidly and economically the geology of large areas (Saunders et al, 1973). Although it was found some geochemical anomalies proximal to known petroleum occurrences, others did not appear related. In no case could an absolute cause-and-effect relationship be demonstrated. Numerous other studies have used remotely sensed data for mapping regional structural patterns and geochemical evaluations of surface anomalies. In comprehensive study using space imagery for petroleum exploration of the Anadarko Basin, it was concluded that using space imagery could reduce the cost of an exploration program (Collins et al, 1975).

In studying the Patrick Draw area of Wyoming, satellite imagery was used, geochemical analyses of surface anomalies, and statistics to show a statistically significant correlation between an interpreted anomaly and known accumulations of oil and gas (Froman, 1976). It was attempted to correlate surface geochemical anomalies detectable on satellite imagery with petroleum occurrences in several locations in Wyoming (Marrs et al, 1977).

Because of the novelty of the technology, along with the varying and sometimes questionable results, many individuals involved in petroleum exploration have shown limited interest in investigating the usefulness of these techniques. If, however, a remote sensing methodology could be developed, one that not only provides a fast accurate method of mapping anomalous geologic structure, but also indicates possible petroleum accumulation by means of a statistical analysis, the costs of an exploration program could be reduced (Ricky, 1982).

Spectral signatures of hydrocarbon bearing materials have characterized absorption at 1.73 and 2.31 μm was explained. The basis of HC mapping process was presented by identifying the unique absorption features for HC material (Clutis, 1989).

Detection of onshore hydrocarbon micro seepages by remote sensing techniques was studied. It was found that hydrocarbon-induced surface alterations of soil and sediments and associated anomalous vegetation that can be identified from remote sensing imagery are reduction of ferric iron (red bed bleaching), conversion of mixed-layer clays and feldspars to kaolinite, increase of carbonate content and anomalous spectral reflectance of vegetation (Yang et al, 2000).

Most researchers working in the field have used 2.31 μm for hyperspectral remote sensing of detecting hydrocarbons. The 1.73 μm feature is very close to a major water absorption maximum but the potential of the 1.73 μm feature for direct detection of HC bearing materials was focused (Höring et al, 2001).

Indexing an algorithm for hyperspectral detection of hydrocarbons was studied and tested. It was demonstrated that the generated algorithm can be used for efficiently detecting HCs. Tests also showed that the HC index derived from the absorption feature 1.73 μm processes even if this feature appears only weakly in the pixel spectra. Besides, HC-bearing materials and oil contaminated ground could be detected and located using HC index images (Kuhn et al, 2002).

Developing a contextual algorithm for detection of mineral alteration halos with hyperspectral remote sensing was studied. It was concluded that the combination of spectral and spatial information in remote sensing images can be considered as a successful method (Jong et al, 2004).

ASTER utility in HC detection with its related mineral alteration was tested. It is documented that ASTER is a cheap and efficient tool for mapping geochemical anomalies related to hydrocarbon seepage (Staskowski, 2004).

In determining anomalous zones by training the classification of satellite imagery with spectral inputs of samples collected over previously defined areas of HC micro seepage was successfully tested. The result of this study showing the clay mineral distribution over anomalous zone supported the outputs (Kahn, 2006).

HC-induced mineral alteration was mapped using ASTER data. Results demonstrated that band ratios of 2 /1 and 4 /8 can discriminate bleached red beds and secondary carbonate minerals due to HC seepage (Fu et al, 2007).

The results of two pixel-based classifications was discussed, namely minimum distance to class means (MDC) and spectral angle mapper (SAM) that have been carried out on hyperspectral imagery acquired over seepage areas. It was found that at best; only 48% and 29% of the pixels that respectively contain crude oil and seepage-related bare soil could be detected, with the inclusion of many false anomalies. Confusion mainly results from the physical characteristics of the anomalies, as these are not unique to seepages. It is concluded that remote sensing of natural hydrocarbon seepages can be improved by image processing algorithms that used spatial information (Van der Werff et al, 2007).

For the evaluation of uranium mineralizing process and looking for new prospect area of uranium deposits , HC leakage induced anomalies were identified such as red bed bleaching was discussed, ferrous iron enrichment and clay mineral alteration using Landsat-7 /ETM+ data processing techniques in the west slope of Songliao basin in China. Basically three enhancement methods were applied; Principle Component Analyses (PCA), band ratio and false color composition to the images and the distribution of tone anomaly of images is consistent with the field data in most area (Zhang et al, 2007).

In 2008, the hypothesis that chemical and mineralogical alterations in rocks and soils are related to hydrocarbon (HC) micro seepages above some of the major oil fields was tested. the mineralogical, geochemical, and carbon isotope supportive field data is mapped by Hyperion image sensors in which alterations that appear to be associated with hydrocarbon micro seepages in the Patrick Draw area of Wyoming (Kahn et al, 2008) .

HC micro seepages in Brazil was characterized, using geo-statistical analysis of regional hydrocarbon geochemical data yielded from soil samples and digital processing of Enhanced Thematic Mapper plus (ETM+/Landsat7 satellite) and Advanced Spaceborne Thermal Emission and Reflection Radiometer imagery

(ASTER/Terra satellite). Indirect indicators of HC micro seepage was studied and band algorithms were developed then classification methods to the satellite images to detect anomalies were applied. Results show that ASTER data possesses excellent potential in onshore exploration of hydrocarbons in Brazil (Lammoglia et al, 2008). Determination the affects of diverse arrays of chemical and mineralogical changes in rocks and soils due to HC micro seepages was tried. To investigate sandstone color alteration patterns, spectroscopy, and ASTER multispectral remote sensing and Synthetic Aperture Radar (SAR) data were used as well as geochemical analyses of selected samples. Using ASTER satellite images and SAR data, the altered areas were identified and mapped (Petrovic et al, 2008).

2.3 REMOTE SENSING REVIEW

Remote sensing can be broadly defined as the collection and interpretation of information about an object, area, or an event without being in physical contact with the object. Aircraft and satellites are the common platforms for remote sensing of the earth and its natural resources. (http://www.aaas.org/page/satellite-imagery-analysis-environmental-monitoring-turkmenbashi-turkmenistan, 2014).

2.3.1 Electromagnetic Energy

The electromagnetic spectrum (EM) is the continuous range of electromagnetic radiation, extending from gamma rays (highest frequency and shortest wavelength) to radio waves (lowest frequency and longest wavelength) and including visible light. The common EM spectrum can be divided into seven different regions as shown in Fig (2.1) a and b:

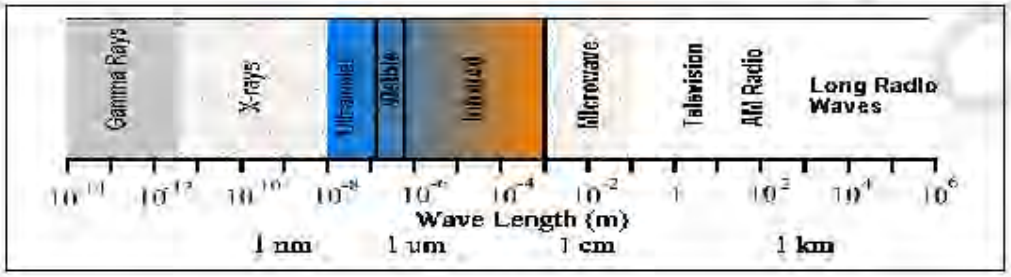

(a)

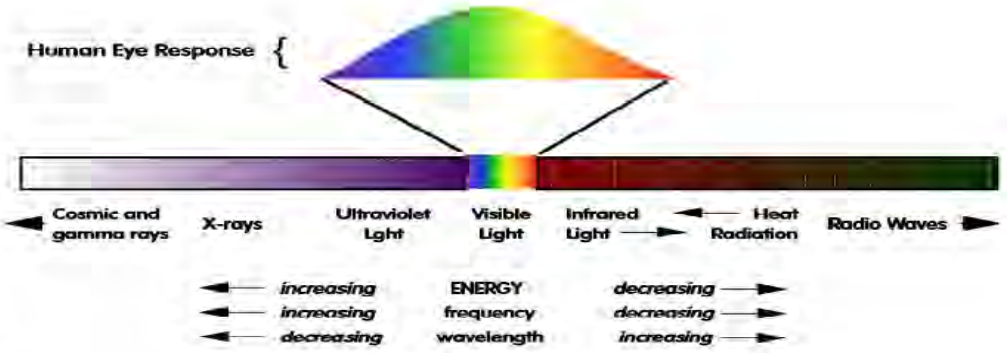

(b)

Figure 2.1: Electromagnetic (EM) spectrum range
(http://www.physics.uc.edu/~sitko/ReflectanceSpectroscopy.pdf, 2014)

Remote sensing involves the measurement of energy in many parts of the electromagnetic (EM) spectrum. A spectral band is defined as a discrete interval of the EM spectrum. For example the wavelength range of 0.4 μm to 0.5 μm (μm = micrometers or 10^{-6} m) is one spectral band. Satellite sensors have been designed to measure responses within particular spectral bands to enable the discrimination of the major Earth surface materials. Scientists will choose a particular spectral band for data collection depending on what is required to be examined (http://www physics.uc.edu /~sitko/ReflectanceSpectroscopy.pdf, 2014).

2.3.2 Reflection and Absorption

When radiation from the Sun reaches the surface of the Earth, some of the energy at wavelengths is absorbed and the rest of the energy is reflected by the surface material. The only two exceptions to this situation are if the surface of a body is a perfect reflector or a true black body. The occurrence of these surfaces in the natural world is very rare. In the visible region of the EM spectrum, the feature we describe as the color of the object is the visible light that is not absorbed by that object. In the case of a green leaf, for example, the blue and red wavelengths are absorbed by the leaf, while the green wavelength is reflected and detected by our eyes. In remote sensing, a detector measures the electromagnetic (EM) radiation that is reflected back from the Earth's surface materials (http://www.cem.msu. edu/~cem 924sg/Topic11.pdf, 2014).

2.3.3 Sensors

A sensor is a device that measures and records electromagnetic energy. Sensors can be divided into two groups as shown in Fig (2.2). Passive sensors depend on an external source of energy, usually the sun, and the most common passive sensor is the photographic camera. Active sensors have their own source of energy; an example would be a radar gun. These sensors send out a signal and measure the amount reflected back. Active sensors are more controlled because they do not depend upon varying illumination conditions (http://iit.edu/arc/workshops/pdfs/SENSORS.pdf).

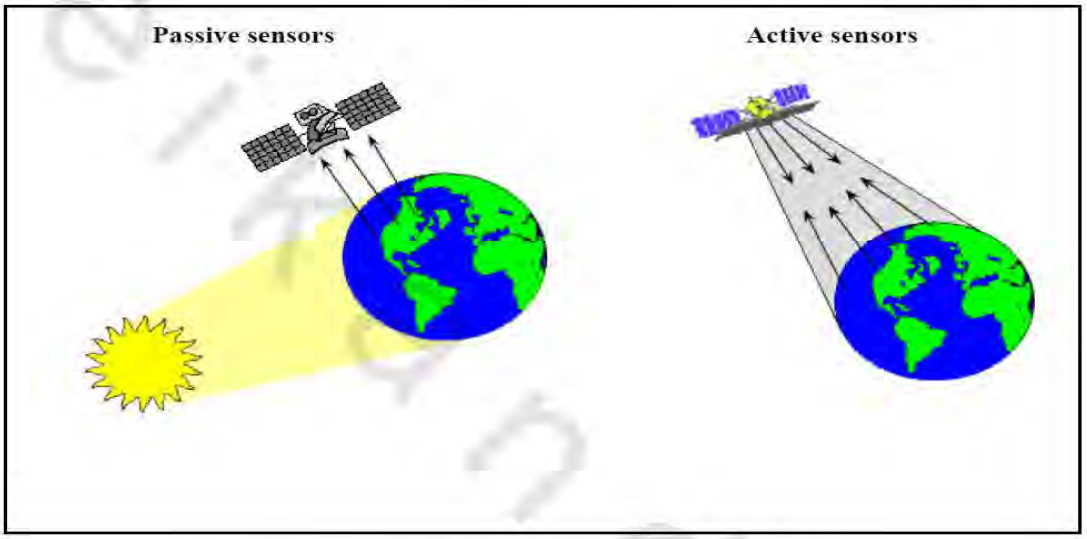

Figure 2.2: Active and Passive sensors
(http://iit.edu/arc/workshops/pdfs/SENSORS.pdf, 2014)

2.3.4 Satellite Sensor Characteristics

The basic function of most satellite sensors is to collect information about the reflected radiation along a pathway, also known as the Field Of View (FOV), as the satellite orbits the Earth. The smallest area of ground that is sampled is called the Instantaneous Field Of View (IFOV). The IFOV is also described as the pixel size of the sensor. The data collected by each satellite sensor can be described in terms of spatial, spectral and temporal resolution (http://irina.eas.gatech.edu/EAS6145_ Spring2013 /Lecture1. pdf, 2014).

2.3.4.1 Spatial Resolution

The spatial resolution (also known as ground resolution) is the ground area imaged for the instantaneous field of view (IFOV) of the sensing device. Spatial resolution may also be described as the ground surface area that forms one pixel in the satellite image. The IFOV or ground resolution of the Landsat Thematic Mapper (TM) sensor, for example, is 30 m (http://www.nrcan.gc.ca/earth-sciences/geomatics/satellite-imagery-air-photos/ satellite -imagery-products/educational-resources/9347, 2014).

2.3.4.2 Temporal Resolution

Temporal resolution is a measure of the repeat cycle or frequency with which a sensor revisits the same part of the Earth's surface. The frequency will vary from several times per day, for a typical weather satellite, to 8-20 times a year for a moderate ground resolution satellite, such as Landsat TM. The frequency characteristics will be determined by the design of the satellite sensor and its orbit and this will be discussed (http://www.nrcan.gc.ca/earth-sciences/geomatics/satellite-imagery-air-photos/satellite - imagery -products/educational-resources/9347, 2014).

2.3.4.3 Spectral Resolution

The spectral resolution of a sensor system is the number and width of spectral bands in the sensing device. The simplest form of spectral resolution is a sensor with one band only, which senses visible light. A sensor with three spectral bands in the visible region of the EM spectrum would collect similar information to that of the human vision system (http://www.nrcan.gc.ca/earth-sciences/geomatics/satellite-imagery-air-photos/satellite-imagery-productseducational-resources/9347, 2014).

2.3.5 Common Satellites Used For Oil Exploration

In the earliest days of oil exploration, the science was little more than the search for natural seepages of oil with the naked eye–find where it was already rising to the surface and drill until you struck the source of the leak. The success rate of the seepage method was about 10%. At that rate, it would be difficult to impossible for oil

producers to keep pace with the growing demand for oil. Now, with the help of modern technology including satellite imagery, the success rate of oil exploration runs about 50% as recorded by BP .There are various satellites used for oil exploration different from other satellites to detect specific objects that will be recorded as oil indicator. This section is derived to summarize the properties of these satellites. (http://blog. urthecast.com/education-tag/the-use-of-satellite-imagery-in-oil-reserve-exploration).

2.3.5.1 Landsat

Since 1972, Landsat satellites have continuously acquired space-based images of the Earth's land surface, coastal shallows, and coral reefs. The Landsat Program, a joint effort of the U.S. Geological Survey (USGS) and the National Aeronautics and Space Administration (NASA), was established to routinely gather land imagery from space. NASA develops the remote-sensing instruments and spacecraft, then launches and validates the performance of the instruments and satellites. The USGS then assumes ownership and operation of the satellites, in addition to managing all ground reception, data archiving, product generation, and distribution. The result of this program is a long-term record of natural and human-induced changes on the global landscape as shown in table 2.1 (http://pubs.usgs.gov/fs/2010/3026/pdf/FS2010-3026.pdf, 2014).

Table 2.1: Landsat Series properties (http://uregina.ca/piwowarj/Satellites/ Landsat. html, 2014).

Platform	Lifetime (design)	Altitude	Equator Crossing	Adjacent Orbits	Repeat Coverage	Sensors
Landsat 1	1972-1978 (1 year)	912 km	8:50 a.m.	1 day	18 days	RBV, MSS
Landsat 2	1975-1982 (1 year)	912 km	9:08 a.m.	1 day	18 days	RBV, MSS
Landsat 3	1978-1983 (1 year)	912 km	9:31 a.m.	1 day	18 days	RBV, MSS
Landsat 4	MSS: 1982-1987 TM: 1982-1999 (3 years)	705 km	9:45 a.m.	7 days	16 days	MSS, TM
Landsat 5	1984-1999 (3 years)	705 km	9:45 a.m.	7 days	16 days	MSS, TM
Landsat 6	1993 (6 years)	705 km	10:00 a.m.	7 days	16 days	MSS, ETM
Landsat 7	1999-present (6 years)	705 km	10:00 a.m.	7 days	16 days	ETM+

The primary sensor onboard Landsat 1, 2, and 3 was the Multispectral Scanner (MSS), with an image resolution of approximately 80 meters in four spectral bands ranging from the visible green to the near-infrared (IR) wavelengths as discussed in table 2.

Table 2.2: Landsat Sensors (http://uregina.ca/piwowarj/Satellites/Landsat.html, 2014).

Sensor	Resolution (m)	Swath Width (km)	Sensor Channels	Spectral Bands (µm)	Example
Return Beam Vidicon (RBV)	80 (LS1,2) 30 (LS3)	185	RBV1	0.475-0.575 (green)	RBV3 image of Cape Canaveral, Florida
			RBV2	0.580-0.680 (red)	
			RBV3	0.690-0.830 (near IR)	
Multispectral Scanner (MSS)	80	185	MSS4	0.5-0.6 (green)	MSS image of Hamilton, Ontario (June 21, 1984)
			MSS5	0.6-0.7 (red)	
			MSS6	0.7-0.8 (near-IR)	
			MSS7	0.8-1.1 (near-IR)	
Thematic Mapper (TM)			TM1	0.45-0.515 (blue)	TM image of Hamilton, Ontario (September 20, 1985)
			TM2	0.525-0.605 (green)	
	30	185	TM3	0.63-0.69 (red)	
			TM4	0.76-0.90 (near-IR)	
			TM5	1.55-1.75 (mid-IR)	
			TM7	2.08-2.35 (mid-IR)	
	120	185	TM6	10.4-12.5 (thermal IR)	
Enhanced Thematic Mapper (ETM+)	15	185	ETM+8	0.520-0.900 (pan)	First public Landsat 7 ETM+ image: Southeastern South Dakota (April 18, 1999)
			ETM+1	0.45-0.515 (blue)	
			ETM+2	0.525-0.605 (green)	
	30	185	ETM+3	0.63-0.69 (red)	
			ETM+4	0.75-0.90 (near-IR)	
			ETM+5	1.55-1.75 (mid-IR)	
			ETM+7	2.09-2.35 (mid-IR)	
	60	185	ETM+6	10.4-12.5 (thermal IR)	

The improved Thematic Mapper (TM) sensors onboard Landsats 4 and 5 were designed with several additional bands in the shortwave infrared (SWIR) part of the spectrum; improved spatial resolution of 30 meters for the visible, near-IR, and SWIR bands; and the addition of a 120-meter thermal-IR band. Landsat 7 carries the Enhanced Thematic Mapper Plus (ETM+), with 30-meter visible, near-IR, and SWIR bands, a 60-meter thermal band, and a 15-meter panchromatic band as shown in table 2.3 (USGS, 2013).

Table 2.3: TM and ETM+ band designations.(http://uregina.ca/piwowarj/Satellites/Landsat.html, 2014).

Spectral bands	Wavelength (micrometers)	Resolution (meters)	Use
Band 1–blue-green	0.45–0.52	30	Bathymetric mapping; distinguishes soil from vegetation; deciduous from coniferous vegetation.
Band 2–green	0.52–0.61	30	Emphasizes peak vegetation, which is useful for assessing plant vigor.
Band 3–red	0.63–0.69	30	Emphasizes vegetation slopes.
Band 4–reflected IR	0.76–0.90	30	Emphasizes biomass content and shorelines.
Band 5–reflected IR	1.55–1.75	30	Discriminates moisture content of soil and vegetation; penetrates thin clouds.
Band 6–thermal	10.40–12.50	120	Useful for thermal mapping and estimated soil moisture.
Band 7–reflected IR	2.08–2.35	30	Useful for mapping hydrothermally altered rocks associated with mineral deposits.
Band 8–panchromatic (Landsat 7)	0.52–0.90	15	Useful in "sharpening" multispectral images.

2.3.5.2 Indian Remote Sensing Satellites (IRS)

The Indian Space program has the goal of harnessing space technology for application in the areas of communications, broadcasting, meteorology and remote sensing. The important milestones crossed so far are Bhaskara-1 and 2 (1979) the experimental satellites, which carried TV Cameras and Microwave Radiometers. The Indian Remote Sensing (IRS) Satellite was the next towards the National operational satellites, which directly generates resources information in a variety of application areas such as forestry, geology, agriculture and hydrology. IRS -1A/1B, carried Linear Imaging Self Scanning sensors LISS-I & LISS-II (Table 2.4). IRS-P2 was launched in

October 1994 on PSLV-D2, an indigenous launch vehicle. IRS-1C, was launched on December 28, 1995, which carried improved sensors like LISS-III, WiFS, PAN Camera, etc. Details of IRS series platforms are given in the following section. IRS-P3 was launched into the sun synchronous orbit by another indigenous launch vehicle PSLV - D3 on 21.3.1996 from Indian launching station (https://www.academia.edu/6242977 /Platform_and_Sensors).

Table 2.4: IRS Satellites Characteristics (http://uregina.ca/piwowarj/Satellites /IRS. html, 2014).

Platform	Lifetime (design)	Altitude	Equator Crossing	Adjacent Orbits	Repeat Coverage	Sensors
IRS-1A, 1B	1A: 1988-1995 1B: 1991-present (3 years)	904 km	10:30 a.m.	1 day	22 days	LISS-I LISS-II
IRS-1C, 1D	1995-present 1997-present (5 years)	817 km	10:30 a.m.	1 day	24 days 5 days 5 days	LISS-III PAN WiFS
RESOURCESAT-1	2003-present (5 years)	817 km	10:30 a.m.		5-24 days	LISS-IV LISS-III AWiFS

Table 2.5: IRS Satellites Sensors (http://uregina.ca/piwowarj/Satellites/IRS.html, 2014).

Sensor	Resolution (m)	Swath Width (km)	Sensor Channels	Spectral Bands (µm)	Example
Linear Imaging Self-Scanning System I (LISS-I)	72	148	LISS-I-1 LISS-I-2 LISS-I-3 LISS-I-4	0.45-0.52 (blue) 0.52-0.59 (green) 0.62-0.68 (red) 0.77-0.86 (near IR)	
Linear Imaging Self-Scanning System II (LISS-II)	36	74	LISS-II-1 LISS-II-2 LISS-II-3 LISS-II-4	0.45-0.52 (blue) 0.52-0.59 (green) 0.62-0.68 (red) 0.77-0.86 (near IR)	
Linear Imaging Self-Scanning System III (LISS-III)	23 50	142 148	LISS-III-2 LISS-III-3 LISS-III-4 LISS-III-5	0.52-0.59 (green) 0.62-0.68 (red) 0.77-0.86 (near IR) 1.55-1.70 (mid-IR)	Southern Iran
	6	70	PAN	0.5-0.75	Toronto, Ontario
High Resolution Linear Imaging Self-Scanning System IV (LISS-IV)	5.8	24 - 70	LISS-IV-2 LISS-IV-3 LISS-IV-4	0.52-0.59 (green) 0.62-0.68 (red) 0.77-0.86 (near IR)	
Wide Field Sensor (WiFS)	188	774	WiFS-1 WiFS-2	0.62-0.68 (red) 0.77-0.86 (near IR)	Appalacian Mountains in Tennessee
Advanced Wide Field Sensor (AWiFS)	56-70	370-740	AWiFS-1 AWiFS-2 AWiFS-3 AWiFS-4	0.52-0.59 (green) 0.62-0.68 (red) 0.77-0.86 (near IR) 1.55-1.70 (mid-IR)	

2.3.5.3 ASTER

The Advanced Space borne Thermal Emission and Reflection Radiometer (ASTER) is an imaging instrument onboard Terra, the flagship satellite of NASA's Earth Observing System (EOS) launched in December 1999. ASTER data is used to create

detailed maps of land surface temperature, reflectance, and elevation. The coordinated system of EOS satellites, including Terra, is a major component of NASA's Science Mission Directorate and the Earth Science Division. The goal of NASA Earth Science is to develop a scientific understanding of the Earth as an integrated system, its response to change, and to better predict variability and trends in climate, weather, and natural hazards (http://asterweb.jpl.nasa.gov/).

Table 2.6: ASTER Satellites Characteristics (http://uregina.ca/piwowarj/Satellites /TerraAqua.html#aster, 2014).

Characteristic	VNIR	SWIR	TIR
Spectral Range	Band 1: 0.52 - 0.60 µm Nadir looking	Band 4: 1.600 - 1.700 µm	Band 10: 8.125 - 8.475 µm
	Band 2: 0.63 - 0.69 µm Nadir looking	Band 5: 2.145 - 2.185 µm	Band 11: 8.475 - 8.825 µm
	Band 3: 0.76 - 0.86 µm Nadir looking	Band 6: 2.185 - 2.225 µm	Band 12: 8.925 - 9.275 µm
	Band 3: 0.76 - 0.86 µm Backward looking	Band 7: 2.235 - 2.285 µm	Band 13: 10.25 - 10.95 µm
		Band 8: 2.295 - 2.365 µm	Band 14: 10.95 - 11.65 µm
		Band 9: 2.360 - 2.430 µm	
Ground Resolution	15 m	30m	90m
Data Rate (Mbits/sec)	62	23	4.2
Cross-track Pointing (deg.)	±24	±8.55	±8.55
Cross-track Pointing (km)	±318	±116	±116
Swath Width (km)	60	60	60
Detector Type	Si	PtSi-Si	HgCdTe
Quantization (bits)	8	8	12

2.3.5.4 NOAA

The National Oceanographic and Atmospheric Administration (NOAA) sent the first of a series of NOAA satellites into orbit in 1970. These satellites move in solar synchronous orbits about 850 km above the Earth and scan the entire Earth in twenty-four hours.

As the NOAA is equipped with both a visible and a near infrared channel, it can also be used for small-scale mapping of vegetation. The daily transects occur at the same local time, making it possible to put together cloudless images based upon several days sensing (http://www.esa.int/SPECIALS/Eduspace_EN/SEMDY3Z2OF_0.html, 2014).

Orbit: sun-synchronous, 833 km altitude

Swath width: 2400 km

Resolution: 1.1 km at nadir

Table 2.7: NOAA Satellites Characteristics (http://uregina.ca/piwowarj/Satellites/NOAA.html, 2014)

	Equator Crossing Times		
Satellite	**Ascending**	**Descending**	**Service Dates**
TIROS-N	1500	0300	10/19/78 - 01/30/80
NOAA-6	1930	0730	06/27/79 - 11/16/86
NOAA-7	1430	0230	08/24/81 - 06/07/86
NOAA-8	1930	0730	05/03/83 - 10/31/85
NOAA-9	1420	0220	02/25/85 - Present
NOAA-10	1930	0730	11/17/86 - Present
NOAA-11	1340	0140	11/08/88 - 09/13/94
NOAA-12	1930	0730	05/14/91 - stand by
NOAA-14	1340	0140	12/30/94 - Present
NOAA-15	1930	0730	05/13/98 - Present
NOAA-16	1400	0200	21/09/00 - Present
NOAA-17	2200	1000	24/06/02 - Present
NOAA-18	1400	0200	20/05/05 - Present

Table 2.8: Advanced Very High Resolution Radiometer (AVHRR) (http:// uregina .ca/ piwowarj/ Satellites/NOAA.html, 2014).

Band #	NOAA-6,8,10 (µm)	NOAA-7,9,11,12,14,15,16,17,18 (µm)	Spectral Region
1	0.58 - 0.68	0.58 - 0.68	visible red
2	0.725 - 1.10	0.725 - 1.10	near-IR
3	3.55 - 3.93	3.55 - 3.93	thermal-IR
4	10.50 - 11.50	10.3 - 11.3	thermal-IR
5	band 4 repeated	11.5 - 12.5	thermal-IR

2.3.5.5 MODIS

MODIS (or Moderate Resolution Imaging Spectroradiometer) is a key instrument aboard the Terra (EOS AM) and Aqua (EOS PM) satellites. Terra's orbit around the Earth is timed so that it passes from north to south across the equator in the morning, while Aqua passes south to north over the equator in the afternoon. Terra MODIS and Aqua MODIS are viewing the entire Earth's surface every 1 to 2 days, acquiring data in 36 spectral bands, or groups of wavelengths ,as shown in table 2.8. These data will improve our understanding of global dynamics and processes occurring on the land, in the oceans, and in the lower atmosphere. MODIS is playing a vital role in the development of validated, global, interactive Earth system models able to predict global change accurately enough to assist policy makers in making sound decisions concerning the protection of our environment (http://modis.gsfc.nasa.gov/about/).

Table 2.9: MODIS Satellites Characteristics (http://uregina.ca/piwowarj/Satellites /TerraAqua.html, 2014)

Orbit:	705 km, 10:30 a.m. descending node (Terra) or 1:30 p.m. ascending node (Aqua), sun-synchronous, near-polar, circular
Scan Rate:	20.3 rpm, cross track
Swath Dimensions:	2330 km (cross track) by 10 km (along track at nadir)
Telescope:	17.78 cm diam. off-axis, a focal (collimated), with intermediate field stop
Size:	1.0 x 1.6 x 1.0 m
Weight:	228.7 kg
Power:	162.5 W (single orbit average)
Data Rate:	10.6 Mbps (peak daytime); 6.1 Mbps (orbital average)
Quantization:	12 bits
Spatial Resolution:	250 m (bands 1-2) 500 m (bands 3-7) 1000 m (bands 8-36)
Design Life:	6 years

2.3.6 Spectral Signatures of Natural and Human-Made Materials

Remote sensing makes use of visible, near infrared and short-wave infrared sensors to form images of the earth's surface by detecting the solar radiation reflected from targets on the ground. Different materials reflect and absorb differently at different wavelengths as shown in Fig (2.3). Thus, the targets can be differentiated by their spectral reflectance signatures in the remotely sensed images.

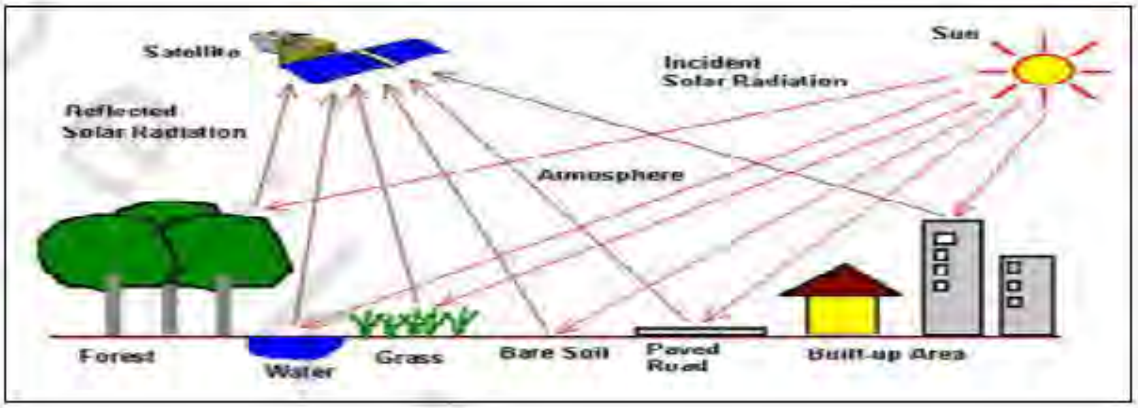

Figure 2.3: Satellite interaction with earth targets (http://www.nrcan.gc.ca/earth-sciences/geomatics/satellite-imagery-air-photos/satellite-imagery-products/educational-resources/9303)

2.3.6.1 Spectral Reflectance Signature

When solar radiation hits a target surface, it may be transmitted, absorbed or reflected. Different materials reflect and absorb differently at different wavelengths. The reflectance spectrum of a material is a plot of the fraction of radiation reflected as a function of the incident wavelength and serves as a unique signature for the material. In principle, a material can be identified from its spectral reflectance signature if the sensing system has sufficient spectral resolution to distinguish its spectrum from those of other materials as shown in Fig (2.4). (http://www.nrcan.gc.ca/earth-sciences/geomatics/satellite-imagery-photos/satellite-imagery-products/educational-resources/9303).

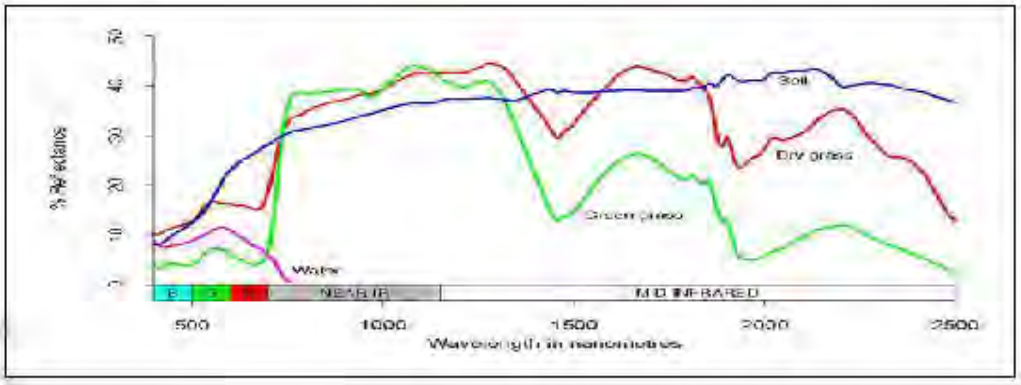

Figure 2.4: spectral reflectance of objects
(http://staff.aub.edu.lb/~webeco/rs%20lectures.htm, 2014)

The reflectance of clear water is generally low. However, the reflectance is maximum at the blue end of the spectrum and decreases as wavelength increases. Hence, water appears dark bluish to the visible eye. Turbid water has some sediment suspension that increases the reflectance in the red end of the spectrum and would be brownish in appearance. The reflectance of bare soil generally depends on its composition.

2.3.6.2 Color Composite Images

In displaying a color composite image, Fig (2.5), three primary colors (red, green and blue) are used. When these three colors are combined in various proportions, they produce different colors in the visible spectrum. Associating each spectral band (not necessarily a visible band) to a separate primary color results in a color composite image.

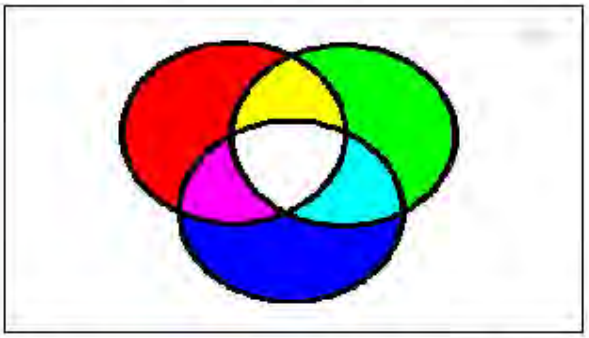

Figure 2.5: Color Composite Images(http://www.crisp.nus.edu.sg
/~research/tutorial/opt_int.htm, 2014)

Many colors can be formed by combining the three primary colors (Red, Green, and Blue) in various proportions.

2.3.6.3 False Color Composite

The display color assignment for any band of a multispectral image can be done in an entirely arbitrary manner. In this case, the color of a target in the displayed image does not have any resemblance to its actual color. The resulting product is known as a false color composite (http://www.crisp.nus.edu.sg/~research/tutorial/opt_int.htm).

2.3.6.4 Natural Color Composite

When displaying a natural color composite image, the spectral bands (some of which may not be in the visible region) are combined in such a way that the appearance of the displayed image resembles a visible color photograph, i.e. vegetation in green, water in blue, soil in brown or grey, etc. Many people refer to this composite as a "true color" composite. However, this term may be misleading since in many instances the colors are only simulated to look similar to the "true" colors of the targets (http://www.crisp.nus. edu.sg/~research/tutorial/opt_int.htm). For example, the bands 3 (red band), 2 (green band) and 1 (blue band) of a AVHRR image, Fig (2.6) can be assigned respectively to the R, G, and B colors for display. In this way, the color of the resulting color composite image resembles closely what the human eyes would observe. There are many possible schemes of producing false color composite images. However, some scheme may be more suitable for detecting certain objects in the image (http://www.crisp.nus.edu.sg/~research/tutorial/opt_int.htm).

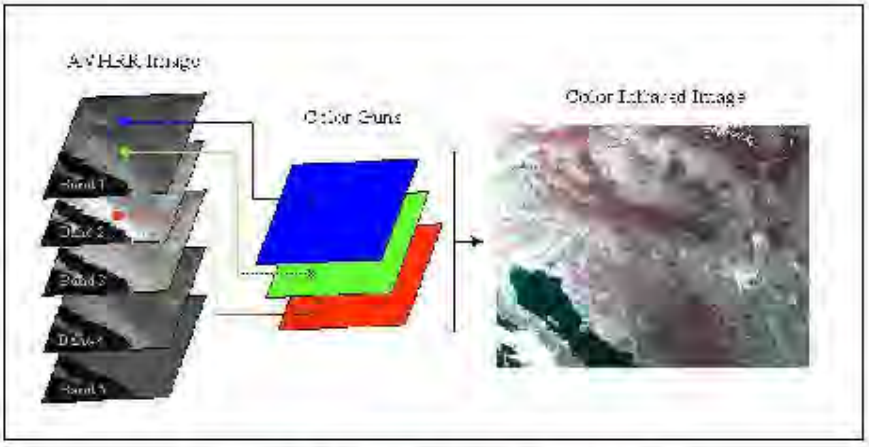

Figure 2.6: Natural Color Composite
(http://www.crisp.nus.edu.sg/~research/tutorial/opt_int.htm)

2.3.7 Image Processing and Analysis

Many image processing and analysis techniques have been developed to aid the interpretation of remote sensing images and to extract as much information as possible from the images. The choice of specific techniques or algorithms to use depends on the goals of each individual project. The key steps in processing remotely sensed data are:

1-Digitizing of Images

2- Image Calibration

3-Geo-Registration

4- Spectral Analysis.

Prior to data analysis, initial processing on the raw data is usually carried out to correct for any distortion due to the characteristics of the imaging system and imaging conditions. Depending on the user's requirement, some standard correction procedures may be carried out by the ground station operators before the data is delivered to the end-user. The image may also be transformed to conform to a specific map projection system. Furthermore, if accurate geographical location of an area on the image needs to be known, Ground Control Points (GCP's) are used to register the image to a precise map (geo-referencing) (http://www.crisp.nus.edu.sg/~research/tutorial/process.htm.).

2.3.7.1 Digitizing of Images

Digital Images is composed of small grid cells called Pixel, as shown in Fig (2.7) each pixel have a value that may express about an object which is composed of multiple connected Pixels. Image digitization is the conversion of an analogue image, such as a photograph, into a series of grid cells. The value of each cell is related to the brightness, color or reflectance at that point.

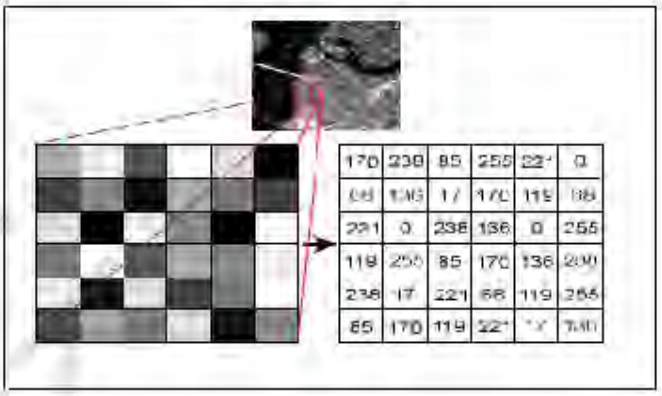

Figure 2.7: pixel values (http://www.crisp.nus.edu.sg/~research /tutorial/process.htm.)

2.3.7.2 Image Enhancement

In order to aid visual interpretation, visual appearance of the objects in the image can be improved by image enhancement techniques such as grey level stretching to improve the contrast and spatial filtering for enhancing the edges (http://www.crisp.nus.edu.sg/~research/tutorial/process.htm, 2014).

2.3.7.3 Image Classification

Different land cover types in an image can be discriminated using some image classification algorithms using spectral features, i.e. the brightness and "color" information contained in each pixel. The spectral features of some areas of known land over types are extracted from the image. These areas are known as the "training areas". Every pixel in the whole image is then classified as belonging to one of the classes depending on how close its spectral features are to the spectral features of the training areas http://www.crisp.nus.edu.sg/~research/tutorial/process.htm, 2014).

2.3.8 Image Interpretation

In order to take advantage and make good use of remote sensing data, it must be able to extract meaningful information from the imagery, as shown in Fig (2.8). This brings to the topic of discussion in this chapter - interpretation and analysis.

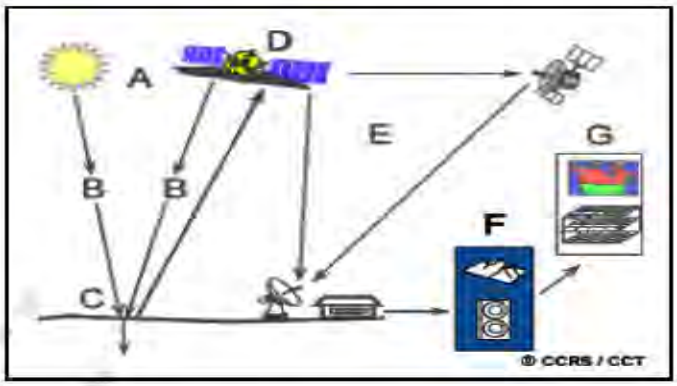

Figure 2.8: Image Interpretation (http://www.crisp.nus.edu.sg/~research /tutorial/process.htm, 2014)

Interpretation and analysis of remote sensing imagery involves the identification and/or measurement of various targets in an image in order to extract useful information about them. Targets in remote sensing images, Fig (2.9) may be any feature or object which can be observed in an image, and have the following characteristics:

The target must be distinguishable; it must contrast with other features around it in the image (http://nature.berkeley. penggong/textbook/chapter7/html/sect71.htm, 2014).

Figure 2.9: Identification of targets

(http://www.crisp.nus.edu.sg/~research/tutorial/process.htm, 2014)

Targets may be a point, line, or area feature. This means that they can have any form, from a bus in a parking lot or plane on a runway, to a bridge or roadway, to a large expanse of water or a field. Much interpretation and identification of targets in remote sensing imagery is performed manually or visually, i.e. by a human interpreter. In many cases this is done using imagery displayed in a pictorial or photograph-type format, independent of what type of sensor was used to collect the data and how the data were collected. In this case, it is referred to the data as being in analog format.

2.3.8.1 Elements of Visual Interpretation

Recognizing targets is the key to interpretation and information extraction. Observing the differences between targets and their backgrounds involves comparing different targets based on any, or all, of the visual elements of tone, shape, size, pattern, texture, shadow, and association. Visual interpretation using these elements is often a part of daily lives, examining satellite images on the weather report, or following high speed chases by views from a helicopter are all familiar examples of visual image interpretation. Identifying targets in remotely sensed images based on these visual elements allows further interpreting and analyzing. The nature of each of these interpretation elements is described below, along with an image example of each.

Figure 2.10: Tone. (http://www.nrcan.gc.ca/earth-sciences/geomatics/satellite-imagery-air-photos/satellite-imagery-products/educationa l-resources/9291, 2014)

Tone refers to the relative brightness or color of objects in an image. Generally, tone is the fundamental element for distinguishing between different targets or features.

Variations in tone also allow the elements of shape, texture, and pattern of objects to be distinguished.

Figure 2.11: Shape. (http://www.nrcan.gc.ca/earth-sciences/geomatics/satellite-imagery-air-photos/satellite-imagery-products/educationa l-resources/9291, 2014)

Shape refers to the general form, structure, or outline of individual objects. Shape can be a very distinctive clue for interpretation. Straight edge shapes typically represent urban or agricultural (field) targets, while natural features, such as forest edges, are generally more irregular in shape, except where man has created a road or clear cuts.

Figure 2.12: Size. (http://www.nrcan.gc.ca/earth-sciences/geomatics/satellite-imagery-air-photos/satellite-imagery-products/educationa l-resources/9291, 2014)

Size of objects in an image is a function of scale. It is important to assess the size of a target relative to other objects in a scene, as well as the absolute size, to aid in the interpretation of that target. A quick approximation of target size can direct interpretation to an appropriate result more quickly

Figure 2.13: pattern.(http://www.nrcan.gc.ca/earth-sciences/geomatics/satellite-imagery-air-photos/satellite-imagery-products/educationa l-resources/9291, 2014)

Pattern refers to the spatial arrangement of visibly discernible objects. Typically an orderly repetition of similar tones and textures will produce a distinctive and ultimately recognizable pattern. Orchards with evenly spaced trees and urban streets with regularly spaced houses are good examples of pattern .(http://www.nrcan.gc.ca/earth-sciences/geomatics/satellite-imagery-air-photos/satellite-imagery-products/educationa l- resources/9291, 2014)

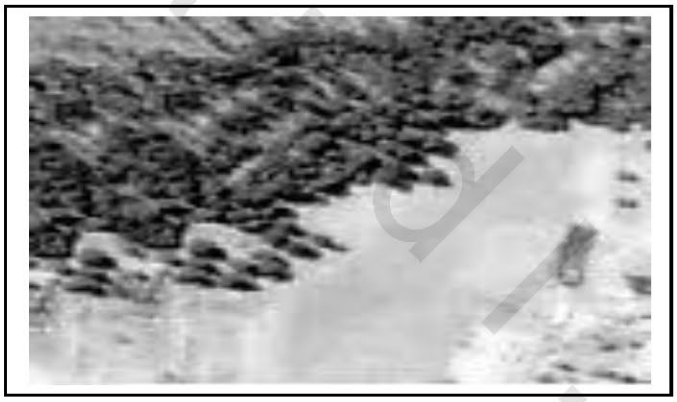

Figure 2.14: texture.(http://www.nrcan.gc.ca/earth-sciences/geomatics/satellite-imagery-air-photos/satellite-imagery-products/educationa l-resources/9291, 2014)

Texture refers to the arrangement and frequency of tonal variation in particular areas of an image. Rough textures would consist of a mottled tone where the grey levels change abruptly in a small area, whereas smooth textures would have very little tonal variation. Smooth textures are most often the result of uniform, even surfaces, such as fields, asphalt, or grasslands.

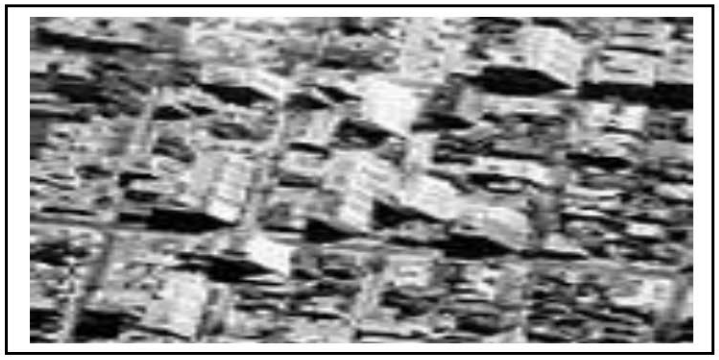

Figure 2.15: Shadow. (http://www.nrcan.gc.ca/earth-sciences/geomatics/satellite-imagery-air-photos/satellite-imagery-products/educationa l-resources/9291, 2014)

Shadow is also helpful in interpretation as it may provide an idea of the profile and relative height of a target or targets which may make identification easier. Shadow is also useful for enhancing or identifying topography and landforms, particularly in radar imagery.

Figure 2.16: Association.(http://www.nrcan.gc.ca/earth-sciences/geomatics/satellite-imagery-air-photos/satellite-imagery-products/educationa l-resources/9291, 2014)

Association takes into account the relationship between other recognizable objects or features in proximity to the target of interest. The identification of features that one would expect to associate with other features may provide information to facilitate identification. In Fig (2.16), commercial properties may be associated with proximity to major transportation routes, whereas residential areas would be associated with schools, playgrounds, and sports fields. In our example, a lake is associated with boats,

a marina, and adjacent recreational land (http://www.nrcan.gc.ca/earth-sciences /geomatics/satellite-imagery-air-photos/satellite-imagery-products/educational-resources /9291, 2014).

2.4 REMOTE SENSING APPLICATIONS FOR OIL EXPLORATION

Exploration for oil and gas has always depended on surface maps of rock types and structures that point directly to, or at least hint at, subsurface conditions favorable to accumulating oil and gas. Thus, looking at surfaces from satellites is a practical, cost-effective way to produce appropriate maps. But verifying the presence of hydrocarbons below surface requires two essential steps: 1) doing geophysical surveys; and 2) drilling into the subsurface to actually detect and extract oil or gas or both.

2.4.1 Formation and Exploration of Oil

Oil and gas result from the decay of organisms - mostly marine plants (especially microscopic algae and similar free-floating vegetation) and small animals such as fish - that are buried in muds that convert to shale. Heating through burial and pressure from the overlying later sediments help in the process. (Coal forms from decay of buried plants that occur mainly in swamps and lagoons which are eventually buried by younger sediments.). The decaying liquids and gases from petroleum source beds, dominantly shale after muds convert to hard rock, migrate from their sources to become trapped as shown in Fig (2.17) (http://hotcopper.com.au/threads /geology-lesson-1481441 /#.VA5TQckT81E, 2014).

The oil and gas must migrate from deeper source beds into suitable reservoir rocks. These are usually porous sandstones, but limestones with solution cavities and even fractured igneous or metamorphic rocks can contain openings into which the petroleum products accumulate.

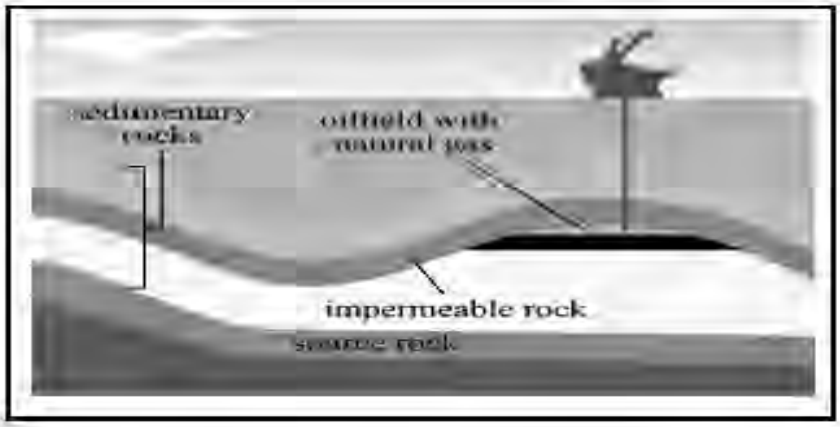

Figure 2.17: Oil Formation and extraction (http://www.hk-phy.org/energy/power/print/source_is_print_e.html, 2014)

An essential condition: the reservoir rocks must be surrounded (at least above) by impermeable (refers to minimal ability to allow flow through any openings - pores or fractures) rock, most commonly shale. The oil and gas, generally confined under some pressure, will escape to the surface - either naturally when the trap is intersected by downward moving erosion surfaces or by being penetrated by a drill. If pressure is high the oil and/or gas moves of its own accord to the surface but if pressure is initially low or drops over time, pumping is required.

Exploration for new petroleum sources begins with a search for surface manifestations of suitable traps (but many times these are hidden by burial and other factors govern the decision to explore). Mapping of surface conditions begins with reconnaissance, and if that indicates the presence of hydrocarbons, then detailed mapping begins. After the mapping, much of the more intensive exploration techniques depends on geophysical methods (principally, seismic) that can give 3-D constructions of subsurface structural and stratigraphic traps for the hydrocarbons. Then, the potential traps are sampled by exploratory drilling and their properties measured.

2.5 METHODOLOGY

The research methodology is based upon the study and analysis of some cases that used satellite images to find oil accumulations and the study of different oil indicators also the study of the common factors that may increase or decrease of the probability of oil existence, also to develop a system that will act as a guide for users for selecting suitable satellite images for their projects according to the given information about the project area.

2.5.1 Finding Oil from Space

Remote sensing from satellites or aircraft strives to find one or more indicators of surface anomalies. The surface and geochemical expression of petroleum seepage can take many forms:

(1) Anomalous hydrocarbon concentrations in sediment, soil, water, and even atmosphere.

(2) Microbiological anomalies and the formation of *paraffin dirt*.

(3) Anomalous no hydrocarbon gases such as helium and radon.

(4) Mineralogical changes such as the formation of calcite, pyrite, uranium, elemental sulfur, and certain magnetic iron oxides and sulfides.

(5) Clay mineral alterations.

(6) Radiation anomalies.

(7) Geothermal and hydrologic anomalies.

(8) Bleaching of red beds.

(9) geobotanical anomalies.

(10) altered acoustical, electrical, and magnetic properties of soils and sediments (http://tle.geoscienceworld.org/content/19/3/258.extract, 2014).

Landsat, and other space imaging systems, serve as mega-photos that depict large areas, within which clues to subsurface conditions may be evident. In general, most of the obvious structures that have surface expression had been discovered and mapped (to varying extents) over much of the world. Some regions, however, were not adequately mapped even in the 1970s, so that the advent of higher-resolution space imagery proved a boon to energy companies seeking new sources of fossil fuels (http://fas.org/irp/imint/ docs/rst/Sect5/Sect5_5.html, 2104). Sometimes the imagery proved especially sensitive to subtle indications of interior structures. For instance, fractures around structures in known oil/gas fields may extend further, as seen in the coherent space images, than suspected from ground work. Also, drainage patterns at broader scales may reflect control by underlying rocks involved in suitable traps. Vegetation distribution may also disclose signs of structure. All indicators are discernible in space imagery appealed to exploration geologists as another means to survey large areas.

2.5.2 Identification of Potential Oil Sites

The two most useful indicators discernible in airborne or spacecraft remote sensors data are fracture systems (mainly lineaments) which can control or affect the migration of gas and oil to the surface and geochemical alterations of surficial rocks by hydrocarbons which lead to compositional and color changes. In this thesis, we will illustrate these ideas by examining and evaluating some case studies using different types of satellite images to demonstrate the feasibility of direct exploration from space (http://fas.org/irp /imint/docs/rst/Sect5/Sect5_5.html, 2014).

2.5.2.1 Fracture Systems (Lineaments)

A lineament is a linear feature in a landscape which is an expression of an underlying geological structure such as a fault. Typically a lineament will comprise a fault-aligned valley, a series of fault or fold-aligned hills, a straight coastline or indeed a combination of these features. Lineaments are often apparent in geological or

topographic maps and can appear obvious on aerial or satellite photographs. Lineaments can control or affect the migration of gas and oil to the surface. The strategy behind the study of linear features was to look at satellite imagery of a region already established as a petroleum province, giving special attention to guide surface indications of the presence of known underlying fields (http://fas.org/irp/imint/docs /rst/Sect5/Sect5_5.html, 2014).

2.5.2.2 Geochemical Alterations of Surficial Rocks by Hydrocarbons

The rock labeled (A) is a sample from the red beds (sandstones) of Permian age. Next to it (B) is the same material that has been color bleached to yellow-brown by converting iron oxide cement into hydrated iron oxides (analogous to rust), (C) is a gypsum rock (hydrated calcium sulphate). The gray rock (D) is a limestone (calcium carbonate). Both interior rocks appear to be altered equivalents of the primary exterior rocks. In the field, comparable altered rocks can occupy many square miles. Alternation of bed rocks, cause change in geological construction of study area (http://fas.org/irpimint /docs/ rst/Sect5/Sect5_5.html, 2014).

Figure 2.18: oil system rock types
(http://fas.org/irp/imint/docs/rst/Sect5/Sect5_5.html, 2014)

Airborne hyperspectral sensors that were flown over known hydrocarbon leaks (in some settings, called micro seeps) have found that an absorption feature near 2.3 μm (one of several in the near IR) is very sensitive to the amount of a specific component of the hydrocarbons as explained in Fig (2.18) a and b. A ratio of two reflectance values on either side of that absorption feature divided by the value of the decreased

reflectance in the spectral curve at the feature's low point enhances the detectability of the hydrocarbon and quantifies its magnitude.

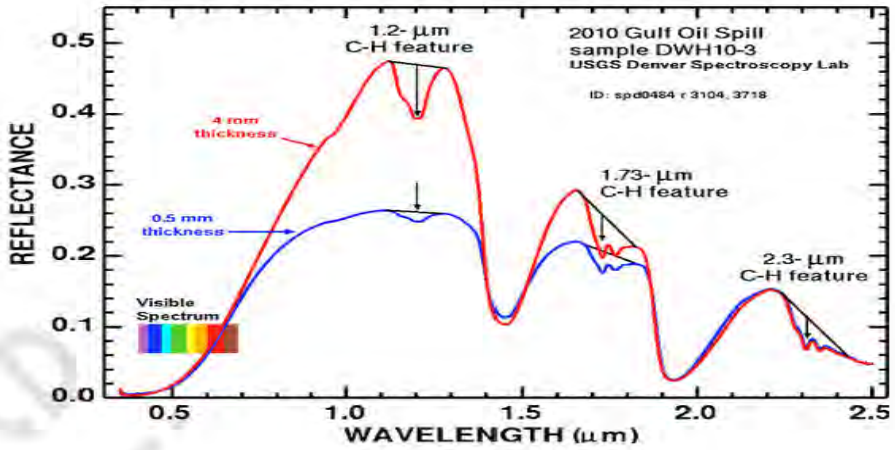

Figure 2.19 (a): A three-wavelength method used to detect hydrocarbons of various sizes to determine areas of thick spilled oil.

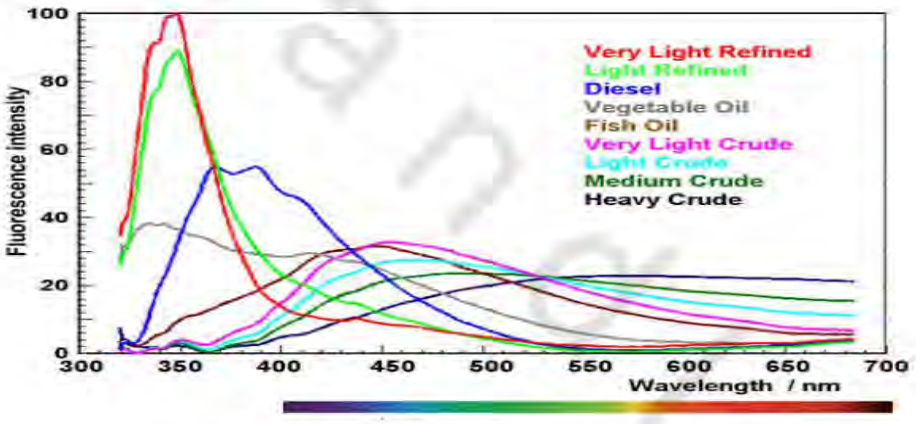

Figure 2.19 (b): Hydrocarbon detection (http://fas.org/irp/imint/docs/rst/Sect5/Sect5_5.html, 2014)

Leaks of oil from fields below the ocean can serve both as an exploration indicator and as a source of environmental damage. Prospecting for oil beneath the open ocean requires some different techniques as well as use of some of the conventional land methods. Oil seeps and slicks can remain intact on the surface and may be detectable in Visible, NIR and radar imagery. The Earth Satellite Corporation has developed SEP – the Seep Enhancement Algorithm - to bring out an oil signature using radar imagery. Fig (2.20) a and b are two examples:

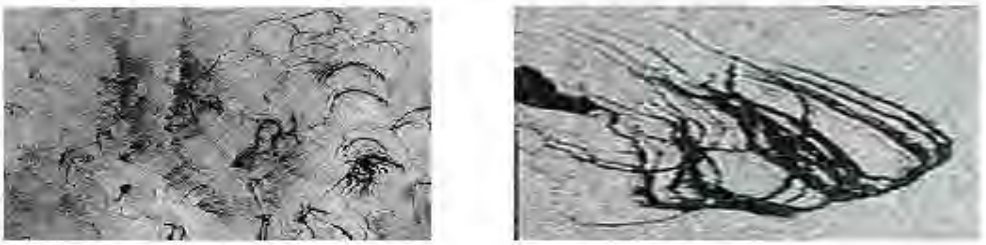

a b

Figure 2.20: Seep Enhancement Algorithm
(http://fas.org/irp/imint/docs/rst/Sect5/Sect5_5.html, 2014)

Oil slicks can be both natural or due to manmade oil spills. The EarthSat image. Fig (2.21) shows a slick off the coast from Kuwait as rendered in a natural color Landsat image.

Figure 2.21: Oil slicks as rendered in a natural color Landsat image
(http://fas.org/irp/imint/docs/rst/Sect5/Sect5_5.html, 2014).

2.5.2.3 Oil Sands Exposed On Surface

The intensity of the economic and political aspects of the availability and costs of oil and gas as still the principal energy sources for such multiple uses as transportation, heating, and petrochemicals is at a, "potentially", highly significant level. Alternate sources of energy, including oil in non-conventional modes of recovery, are being pushed. Two huge potential suppliers are Canada (tar sands) and Venezuela (heavy oil; requires pumping in hot water to release the oil from its host rock). Estimates of

available oil from these types of deposits in Alberta, Canada approach, or may exceed, two trillion barrels (Venezuelan heavy oil is at least one trillion barrels).

Figure 2.22: The Canadian oil sands (http://bestcalgaryhomes.com/9-shocking-oilsands-truths, 2014)

The Canadian oil sands were first discovered in the late 1700s. The sand units outcrop at the surface in the northeast part of the province of Alberta but have a wider distribution subsurface, as seen in the above map.

The Cretaceous sandstones that contain sticky, near-solid bitumens (up to 20%) filling interstitial pores have been called Athabasca Tar Sands or now more commonly Alberta Oil Sands. Here is a surface photo of an outcrop rich in the blackish tar that pervades the rock as discussed in Fig (2.23).

The oil sands after surface removal are further broken up and then extracted from the rock pores by subjecting the material to hot water and other chemicals. A barrel of thick oil requires processing of about a ton of the oil sand (https://apollomapping.com/wp-content/user_uploads/2011/11/NASA_Remote_Sensing_Tutorial_Oil_and_Gas, 2014).

Figure 2.23: surface stripping of the oil sands (https://apollomapping.com/wp-content/user_uploads/2011/11/NASA_Remote_Sensing_Tutorial_Oil_and_Gas, 2014)

2.5.3 An Optical Model for the Interpretation of Remotely Sensed Multispectral Images of Oil Detection

Oil detection and oil type identification can potentially be achieved using data from multispectral optical sensors. However, multispectral images interpretation is challenging, because the spectral signature depends not only on oil optical properties and film thickness, but also on the optical properties of the water column, the incident light distribution and the instrument viewing geometry, a simulator has been developed, starting from an optical model for both clean and polluted surfaces, which makes it possible to analyze variability in the optical signal from an oil-covered water surface. Incident light distributions and viewing configurations have been chosen according to a typical viewing geometry of The Medium Resolution Imaging Spectrometer (MERIS) sensor over a particularly interesting Mediterranean area.

The results, shown in terms of both upwelling radiance and oil-water optical contrast, provide some general rules that may aid interpretation of MERIS data. In particular, the detectability of an oil slick has been shown to depend on oil type and film thickness: very thin oil films are more easily detected at viewing directions near the

sun-glint zone, while very thick films are more likely to be detected at viewing angles away from the sun, for films of intermediate thickness the detectability depends mainly on the oil's specific optical properties. At present, several instruments are available for oil detection, mounted on board of airborne and space platforms: radar, microwave radiometers, laser fluorosensors, and passive optical and thermal infrared sensors.

Each instrument has strengths and limitations, so that the synergistic use of different sensors will improve oil detection capability. Synthetic Aperture Radar (SAR) is the main sensor used in oil detection, as surface oil dampens capillary waves and leads to reduced radar backscattering. This instrument is preferred to optical sensors due to its all-day and all-weather capabilities. However, the application of SAR data to oil detection is limited to a small range of wind speed (1.5-6 m/s). Moreover, monitoring based only on SAR can be problematic because of ambiguities due to other natural phenomena that reduce the SAR signal, and because it cannot provide information that may be used for thickness estimates or oil type identification. Oil is detectable at sea by optical sensors due to its refractive index, which is higher than that of water, and its absorption coefficient, which is stronger than that of water. The optical properties changes vary slightly from oil to oil, and have been widely investigated through laboratory analyses.

2.5.3.1 Oil Optical Properties

Crude and refined oils are characterized mainly by three Inherent Optical Properties (IOP's), which vary slightly from oil to oil and make them detectable at sea by optical sensors (Byfield, 1998):

1. Their refractive index n_o, *"which commonly defined as the ratio of the speed of light in vacuum relative to that in the considered medium"*, higher than that of sea water ($n_w \approx 1.34$).

2. Their coefficient of light absorption $a_o(\lambda)$, typically several order of magnitude stronger than that of water, especially at shorter wavelengths. In particular, laboratory analyses showed that typical oil absorption spectra are characterized by strong

absorption at short wavelengths, with an exponential decay towards longer wave lengths as shown in Fig (2.24) (Wang, 1994).

3. Their solar-induced fluorescence, with fluoresce peaks that vary in width and wavelength position according to oil type, and an exponential decay towards the red and NIR. In particular, lighter oils fluoresce at shorter wavelengths (UV to green), while heavier oils have broader fluorescence spectra, with peak at longer wavelengths.

In particular, four different oils have been considered, each belonging to a different class: diesel (light refined), Forties (light crude), Alaskan (heavy crude) and Heavy Fuel Oil (HFO – heavy refined). The refractive indexes and absorption coefficients are shown in Table 2.10 and Fig (2.24) respectively

Table 2.10: Refractive indexes of the four different oils analyzed (Byfield, 1998)

Oil	Refractive Index
DIESEL (Light refined oil)	1.472
FORTIES (Light crude oil)	1.480
ALASKAN (Heavy crude oil)	1.510
HFO (Heavy refined oil)	1.551

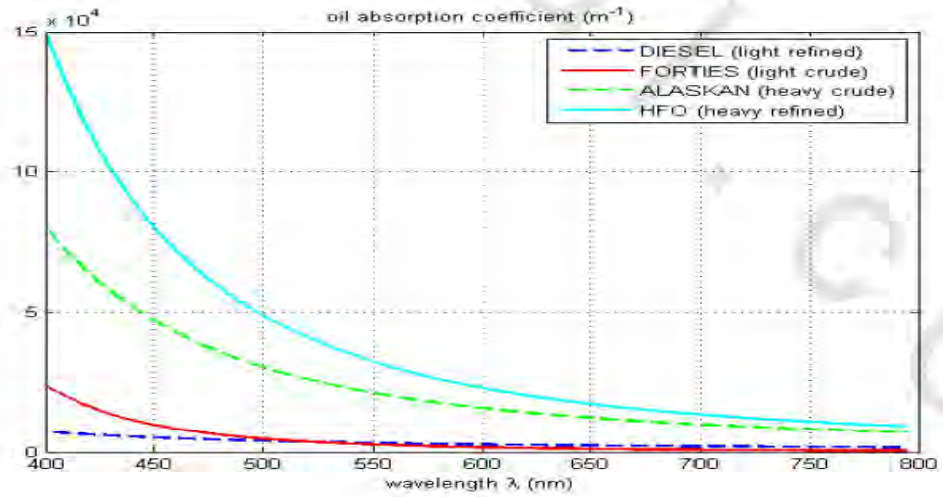

Figure. 2.24 Absorption coefficients of the four different oils analyzed: diesel, Forties, Alaskan, and Heavy Fuel Oil (HFO) (Byfield, 1998).

2.5.3.2 Optical Model of Upwelling Radiance

The clean sea water upwelling radiance at the Top Of Atmosphere (TOA), Lu^{TOA}, can be in general expressed as the sum of three main contributions , as schematized in Fig (2.25) (a): the atmospheric path radiance L_{path}, which has not interacted with the sea water surface and body; the reflected sky radiance contribution L_{sky_refl}, due to the solar radiation scattered by the atmosphere and reflected from the sea surface; the water-leaving radiance L_{wl}, resulting from the interaction of the incident radiation with the sea water's constituents (Byfield, 1998).

In particular, given as assumption that the atmospheric effects have been removed from the remotely-sensed data, the upwelling radiance just above the water surface (i.e. at level 0^+) is

$$Lu\,(0^+;\lambda;\theta_v,\Delta\phi) = L_{sky\_refl}(0^+;\lambda;\theta_v,\Delta\phi) + L_{wl}(0^+;\lambda;\theta_v,\Delta\phi) \quad (2.1)$$

Where λ is the wavelength, θ_v represents the zenithal viewing angle, and $\Delta\phi = \phi s - \phi v$ the difference between the azimuthal viewing and solar angles. The dependence on zenithal solar angle θs is implicit. Here the reflected sky radiance contribution is assumed to include also the sun glint term, which, for a flat surface, corresponds to the viewing direction specular to the direction of the direct incident solar radiation. The terms in Equation (2.1) are considerably influenced by the presence of an oil film onto the sea water surface. In the following paragraphs, we discuss analytical expressions for the upwelling radiance above the water surface, both for clean and oil-covered water, under the assumption of an ideally flat sea water surface.

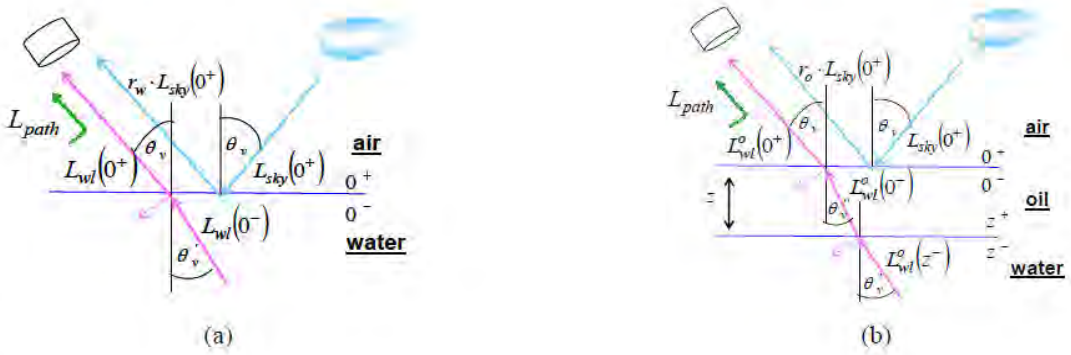

Figure 2.25 Schematization of the upwelling radiance contributions measured by a sensor above a flat sea surface for a clean sea water surface (a) and oil-covered surface (b) (Byfield, 1998).

2.5.3.3 Upwelling Radiance from Clean Sea Water

The water-leaving radiance contribution from clean sea water is obtained starting from the incident downwelling radiance distribution, which is transmitted through the air-water interface and, after the interaction with the sea water's constituents, is partially backscattered in the upward direction and transmitted through the water-air interface. For flat water surface the reflection and transmission of radiance at the air-water interface can simply be solved through the Fresnel's coefficients, and Equation (2.1) can be expressed as:

$$L_u(0^+;\lambda;\theta_v,\Delta\phi) = r_w(\theta_v).L_{sky}(0^+;\lambda;\theta_v,\Delta\phi) + \frac{t_w(\theta'_v).t_{dw}}{n_w^2.(1-r_{uw}.R(0^-;\lambda))}.\frac{R(\theta^-;\lambda)}{Q(0^-;\lambda;\theta_v,\Delta\phi)}.E_d(0^+;\lambda) \quad (2.2)$$

Where:

- $L_{sky}(0^+;\lambda;\theta_v,\Delta\phi)$ represents the incident sky radiance distribution.
- $r_w$and $t_w$are the Fresnel reflection and transmission coefficients at the air-water interface, respectively.
- θ'_vrepresents the refracted zenithal viewing angle under the water surface.

$$\theta'_v = \boldsymbol{sin}^{-1}(\boldsymbol{n_w}.\,\mathbf{sin}(\boldsymbol{\theta_v}))$$

- t_{dw} is the diffuse transmission coefficient for down welling irradiance across the air-water interface.
- $r_{uw}$is the diffuse reflection coefficient for upwelling radiance at the water-air interface.
- $E_d(0^+;\lambda)$is the incident downwelling irradiance
- $Q(0^-;\lambda;\ \theta_v, \Delta\phi)$ *is* the Q factor, defined as the ratio between upwelling irradiance and radiance, thus representing a measurement of the anisotropy of the upwelling radiation:

$$\boldsymbol{Q(0^-;\lambda;\ \theta_v, \Delta\phi) = E_u(0^-;\lambda)/L_u(0^-;\lambda;\ \theta'_v, \Delta\phi)}$$

- $R(\theta^-;\lambda)$ is the subsurface reflectance irradiance, defined as :

$$\boldsymbol{R(\theta^-;\lambda) = E_u(0^-;\lambda)/E_d(0^-;\lambda)}$$

which is a function of the sea water Inherent Optical Properties (IOP's), i.e. absorption and backscattering coefficients, and thus of the Optical Active Parameters (OAPs), i.e. the concentration of sea water optical active constituents (chlorophyll, yellow substance and suspended sediments)

It is worth noting that the term $r_{uw}{\cdot}R(\theta^-;\lambda)$, which takes account of the internal reflection of subsurface upwelling irradiance, is generally negligible at the angles usually used for remote sensing applications.

2.5.3.4 Impact of Surface Oil Film on Upwelling Radiance Distribution

Equation (2.2) is modified by surface oil, as illustrated in Fig (2.25) (b). Concerning the water-leaving radiance contribution, the incident radiation is transmitted through the air-oil interface into the oil, then through the oil layer, and finally through the oil-water interface. As the oil refractive index is higher than that of water, the diffuse transmission coefficient at the air-oil interface is lower than that at the air-water interface. Light is absorbed by the oil film, to an extent dependent on the oil absorption

coefficient and the film thickness. A small amount of radiation is also lost at the oil-water interface due to reflection of the downward radiation, but this loss can be usually considered negligible, compared to the losses due to transmission through the air-oil interface and absorption by the oil film. Within the water column the downwelling radiance is partially backscattered in the upward direction, due to the interaction with the sea water constituents. This upwelling radiance is subsequently transmitted through the water-oil interface, the oil film, where it is again absorbed, and finally the oil-air interface (Mobley, 1999).

Taking account of these processes, the total upwelling radiance from a flat oil-covered sea surface can be expressed analytically as follows:

$$L_u^0(0^+;\lambda;\theta_v,\Delta\phi) = r_0(\theta_v)L_{sky}(0^+;\lambda;\theta_v,\Delta\phi) + \frac{t_0(\theta_v'')t_{wo}(\theta_v')t_{do}t_{dwo}}{n_w^2} e^{-\left(\frac{1}{\overline{\mu_d}}+\frac{1}{\cos\theta_v''}\right).a_0(\lambda).z} \cdot \frac{R(0^-;\lambda)}{Q(0^-;\lambda;\theta_v,\Delta\phi)} . E_d(0^+;\lambda) \qquad (2.3)$$

Where:

- r_0 and t_0 are the Fresnel reflection and transmission coefficients at the air-oil interface, respectively
- θ_v''represents the refracted zenithal viewing angle under the oil-water interface

$$\theta_v'' = sin^{-1}(n_w.\sin(\theta_v)/n_0))$$

- $t_{wo}$is the Fresnel transmission coefficient at the water-oil interface
- θ_v' is the total refracted viewing angle under the oil-water interface (which is equal to the one under the air-water interface for clean sea water, as a result of the consecutive transmissions through the air-oil and oil-water interfaces)
- t_{do} and t_{dwo} are the diffuse transmission coefficients for downwelling irradiance across the air-oil and oil-water interfaces, respectively
- $\overline{\mu_d}$ is the average cosine of downwelling irradiance within the oil layer

- $a_0(\lambda)$ Is the absorption coefficient of the oil and z is the oil film thickness (Mobley, 1999).

2.5.3.5 Definition of Oil-Water Spectral Contrast

As a consequence of the absorption within the oil film and the lower oil transmission coefficient, the water-leaving radiance contribution from an oil-covered surface is lower than the one from a clean surface. However, because of the higher Fresnel reflection at the air-oil interface, the specularly reflected sky radiance contribution is higher for an oil covered surface than for a clean one. Thus, the visibility of oil onto the water surface depends on the balance between the oil-water difference in water-leaving radiance and the corresponding difference in reflected sky radiance. This balance can be expressed in terms of oil-water spectral contrast, which is defined as the net difference in measured upwelling radiance between oil-covered and clean water, normalized with respect to the upwelling radiance from clean water (to reduce the effect of variations in incident light) (Mobley, 1999).

From Equations (2.2) and (2.3), oil-water spectral contrast can be expressed as:

$$c(0^+;\lambda;\theta_v,\Delta\phi) = \frac{L_u^0(0^+;\lambda;\theta_v,\Delta\phi) - L_u(0^+;\lambda;\theta_v,\Delta\phi)}{L_u(0^+;\lambda;\theta_v,\Delta\phi)!} = \qquad (2.4)$$

$$\frac{[r_0 - r_w].L_{sky}(0^+;\lambda) - \left[t_w.t_{dw} - t_0.t_{d0}.t_{wo}.t_{dwo}.e^{-\left(\frac{1}{\overline{\mu_d}} + \frac{1}{\cos\theta_v''}\right).a_0(\lambda).z}\right].\frac{R(0^-;\lambda)}{n_w^2.Q(0^-;\lambda)}.E_d(0^+;\lambda)}{r_w.L_{sky}(0^+;\lambda) + \frac{t_w.t_{dw}}{n_w^2}.\frac{R(0^-;\lambda)}{Q((0^-;\lambda)}.E_{d(0^+;\lambda)}}$$

Equation (2.4) represents the balance between positive contrast arising from specular reflection and negative contrast arising from water-leaving radiance. This balance is influenced by several factors not only the oil optical properties and film thickness but also the sea water's optical properties, the illumination condition and viewing configuration. For example, for thin oil films, a positive contrast is expected at wavelengths where the sky radiance is high, or the subsurface reflectance is low, which is usually the case in the violet and blue range (400-480 nm) and the NIR (beyond 700 nm) respectively. As thickness increases, the exponential term in Equation (2.4) approaches zero, and there is no signal contribution from the water beneath the oil. In

this case, contrast is expected to be negative at wavelengths within the seawater reflectance peak, except for viewing angles that give specular reflection of direct sunlight. In the red and NIR, where $R(0^- ;\lambda)$ is negligible due to the high water absorption coefficient, the contrast should be positive, except when the concentration of scattering particles into the water column is high. For thinner films, a high positive contrast is expected for viewing configurations towards the solar side, regardless of the water properties, as sky radiance is higher in the region surrounding the sun. These expected trends will be confirmed in the following sections, where the results of the simulation of upwelling radiance and oil-water contrast, as well as the analysis of their variability, will be presented (Mobley, 1999).

2.5.3.6 Description of the Oil – On – Water Signature Simulator

In order to model the oil-covered surface upwelling radiance and the oil-water contrast, a simulator has been developed, based on known numerical model, which simulates the clean sea water radiance contribute on according to Equation (2.2). The oil contribution has been subsequently introduced according to Equation (2.3), by using some outputs directly returned by the numerical model and considering the oil optical properties. A schematic of this simulator is shown in Fig (2.26). several quantities are accepted as inputs (Mobley, 1999):

- Sea water's OAPs, i.e. chlorophyll concentration (Cchl), expressed in mg/m^3, absorption coefficient of yellow substance at a reference wavelength Y (m^{-1}) and suspended matter concentration X (g/m^3);
- Incident light distribution, expressed in terms of zenithal solar angle, cloud cover percentage and atmospheric parameters (e.g. sea-level pressure, average horizontal visibility and relative humidity);
- Wind speed w, expressed in m/s, here assumed equal to 0 m/s.

The configuration of the model used here returns the upwelling radiance distribution above a clean water surface for any viewing configuration, with a zenith-angle resolution of 10° and an azimuth-angle resolution of 15°. At the same time, several intermediate quantities are computed (e.g. the incident downwelling irradiance and sky

radiance, the subsurface reflectance irradiance, the Q-factor and the average downwelling cosine). These may be used as inputs for the computation of the signal from water covered with an oil film. For these calculations the oil optical properties and the film thickness need to be specified, as well as the reflection and transmission coefficients at the air-oil and oil-water interfaces.

Here it has been assumed $t_{dwo} = t_{wo} = 1$, which is a good approximation for the light and viewing configuration typical of remote sensing applications ($\theta v \leq 40°$ and $\theta s \leq 80°$)). *to* and *ro* have been computed according to the Fresnel law. Regarding *tdo*, a good approximation is obtained by combining the coefficients computed by considering separately the direct and diffuse components of the downwelling irradiance. In this way it is possible to compute the transmission coefficient for the direct component as the Fresnel's coefficient at the incident solar zenith angle, and the transmission coefficient for the diffuse component as the Fresnel's coefficient at an incident angle equal to the average downwelling cosine (Mobley, 1999).

By varying the inputs of the simulator, it is possible to evaluate the variability of upwelling radiance from an oil-covered surface and calculate the oil-water contrast as a function of several factors.

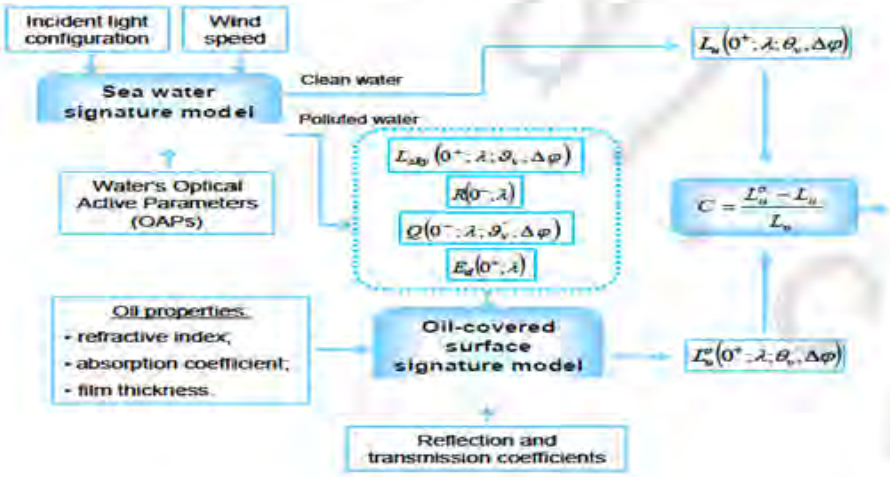

Figure 2.26: Schematization of oil-on-water signature and oil-water contrast simulator (Mobley, 1999).

Finally, remote sensing aids in exploration for oil and gas by:

1) Providing overviews of the regional geologic setting in which oil and gas is being sought.

2) Helping to define existing fold/fault structures.

3) Demarcating linear features that are usually fractures along which hydrocarbons migrate.

4) Detecting alteration of rocks by escaping hydrocarbons.

5) Finding other signatures indicated by fluorescent anomalies in the Ultra Violet and compositional anomalies in the IR.

6) Noting oil directly as leaks, spills, and seepage in the oceans/lakes or on land.

7) Observing environmental damage associated with drilling, pumping, pipeline transfer, and refining of hydrocarbons (Nicholas et al, 2007).

2.6 DOMINANT FACTORS IN USING REMOTE SENSING IMAGES FOR OIL EXPLORATION

According to the study of different scientific researches and projects, the main factors that affect the use or remotely sensed data for oil exploration are:

- Study Area topography
- Geological structure
- Existing auxiliary data
- Selected Satellite images

All the above factors will be explained in the following sections

2.6.1 Study Area Topography

A study area is an area of known geographic extent for which data is analyzed and mapped in a report. The topographic condition of the concession area is an important factor that affects the selection of the suitable satellite images for the area of interest. Different conditions are concluded in this research explaining the best suitable Study area might be (Forests – Deserts - Valleys – Grasslands - Shores – Islands – Sea - Ocean). The main types that are employed in this study are (Deserts – sea – ocean – shores and Grasslands).

2.6.2 Geological Structure

Petroleum geology is the study of origin, occurrence, movement, accumulation, and exploration of hydrocarbon fuels. It refers to the specific set of geological disciplines that are applied to the search for hydrocarbons (oil exploration). (http://en.wikipedia .org/wiki/Petroleum_geology, 2014).

2.6.2.1 Petroleum geological System

The Petroleum System consists of a mature source rock, migration pathway, reservoir rock, trap and seal. Appropriate relative timing of formation of these elements and the processes of generation, migration and accumulation are necessary for hydrocarbons to accumulate and be preserved (http://www.landforms.eu /orkney /Geology /Oil/OIL%20petroleum%20system.htm, 2014).

2.6.2.2 Source Rock Hydrocarbon Generation

The formation of hydrocarbon liquids from an organic rich source rock with kerosene and bitumen to accumulates as oil or gas. Generation depends on some main factors:

- The presence of organic matter rich enough to yield hydrocarbons.
- Adequate temperature.
- The sufficient time to bring the source rock to maturity.
- Pressure and the presence of bacteria and catalysts also affect generation.

Generation is a critical process in the development of a petroleum system and has different phases can be categorized as following:

A. Migration

The movement of hydrocarbons from their source into reservoir rocks and the movement of newly generated hydrocarbons out of their source rock is primary migration, also called expulsion. The further movement of the hydrocarbons into reservoir rock in a hydrocarbon trap or other area of accumulation is secondary migration (http://www.landforms.eu/Orkney/Geology/Oil/OIL%20 petroleum %20system.htm, 2014).

Migration typically occurs from a structurally low area to a higher area in the subsurface because of the relative buoyancy of hydrocarbons in comparison to the surrounding rock. Migration can be local or can occur along distances of hundreds of kilometres in large sedimentary basins, and is critical to the formation of a viable petroleum system.

B. Accumulation

The phase in the development of a petroleum system during which hydrocarbons migrate into and remain trapped in a reservoir.

C. Reservoir

A subsurface body of rock having sufficient porosity and permeability to store and transmit fluids. Sedimentary rocks are the most common reservoir rocks because they have more porosity than most igneous and metamorphic rocks and they form under temperature conditions at which hydrocarbons can be preserved.

D. Seal (Cap Rock)

An impermeable rock that acts as a barrier to further migration of hydrocarbon liquids. Rocks that forms a barrier or cap above and around reservoir rock forming a trap such that fluids cannot migrate beyond the reservoir. The permeability of a seal capable of retaining fluids through geologic time is $\sim 10^{-6}$ to 10^{-8}decries. Commonly shale.

E. Trap

A configuration of rocks suitable for containing hydrocarbons and sealed by a relatively impermeable formation through which hydrocarbons will not migrate. Traps are described as Structural traps and Hydrocarbon traps. Structural traps that form in geologic structures such as folds and faults stratigraphic traps. Hydrocarbon traps that result from changes in rock type or pinch-outs, unconformities, or other sedimentary features such as reefs or buildups (http://www.landforms.eu /orkney /Geology /Oil/OIL %20petroleum %20system.htm,2014).

2.6.3 Existing Auxiliary Data

The following data sets from different sources were used in this thesis:

1. Remote sensing data digital data (different satellite images).

2. Existing geological maps, structure contour maps, and topographical maps.

3. Field survey data of existing well and seismic line locations, as well as GPS survey points (used as GCPs during georeferencing).

4. Surface Digital elevation model data.

5. Hydrocarbonphilous biology data (Bungum et al, 2006).

2.6.4 Satellite Image

Satellite imagery consists of images of earth or other planets collected by artificial satellites. Satellite images have many applications in meteorology, agriculture, geology, forestry, landscape, biodiversity conservation, regional planning, education, intelligence and warfare. Images can be in visible colors and in other spectra. There are also elevation maps, usually made by radar images. Interpretation and analysis of satellite imagery is conducted using specialized remote sensing applications. Some of the first image enhancement of satellite photos was conducted by the U.S. Government and its contractors.

For example ESL Incorporated developed some of the earliest two dimensional Fourier transforms applied to digital image processing to address NASA photos as well as national security applications. Satellite imagery is also used in seismology and oceanography in deducing changes to land formation, water depth and sea bed, by color caused by earthquakes, volcanoes, and tsunamis (Sundberg, 1994).

2.6.4.1 Selecting Suitable Satellite Images

The capacity of satellite imagery to detect anthropogenic impacts on land cover was assessed for different case studies that are included in this section. These range from physical obstructions, such as roads, railways, and pipelines, to direct and indirect ecological impacts, such as changes in vegetation and hydrology. Nenets' perceptions of their territories encompass changes in the quantity and quality of terrestrial and freshwater habitats and campsites that have been used seasonally for centuries. Industrial impacts on land cover were examined at spatial scales from very detailed to coarse.

Very-high-resolution Quickbird-2 imagery revealed the most impacts, but could not detect items like trash that reduce the quality of reindeer pastures. ASTER, SPOT, and Landsat imagery were useful at the broader landscape level. A proper assessment of the overall ecological impacts of hydrocarbon exploitation requires a combination of remote sensing and detailed ground-truthing. Ideally, these efforts should combine scientific and local knowledge from both indigenous herders and non-indigenous industrial workers. (KUMPULA et al , 2009).

The below table shows capacity of imagery to detect different impacts of hydrocarbon exploration in Bovanenkovo, compared to socio-cultural surveys and ground-truthing. Rankings: (–) not visible, (x) visible with effort, (xx) moderately visible, (xxx) clearly visible.

Table 2.11: Capacity of imagery to detect different impacts of hydrocarbon exploration (KUMPULA et al, 2009)

Impact	Socio-cultural Survey	Ground Truthing	Quickbird-2 Panchromatic	Quickbird-2 Multispectral
Small Scale (< 0.09 ha):				
Soil contamination		××	××	-
Removal of top soil and vegetation	×××	×××	×××	××
Industrial waste:				
Metal	××	××	×	-
Glass	××	×	-	-
Concrete	×××	×××	××	×
Wood	×××	×××	×	-
Single off-road vehicle track	××	××	×××	××
Vegetation changes				
Shrubs to graminoids	×	××	×	××
Peatland to graminoids	×	×××	×	××
Revegetated barren ground	×	×××	×	××
Pipelines	×××	×××	×××	××
Power lines	×××	×××	××	×
Drilling towers	×××	×××	×××	××
Trucks/Vehicles	×××	×××	××	×
Roads	×××	×××	×××	×××

Table 2.11: Satellite sensors and their radiometric and spatial resolution (KUMPULA et al, 2009).

Sensor	No Of Channels	Pixel Size(m)	Pixel Area(m^2)	Small Scale (No. of Pixels			Medium Scale (No. of Pixels) 1 ha	Large Scale (No. of Pixels) 10 ha
				0.0025 ha	0.01 ha	0.09 ha		
Quickbird-2 pan	1	0.6 × 0.6	1.2	20.8	83.3	750.0	8333.3	83333.3
Quickbird-2 multi	4	2.4 × 2.4	5.76	4.3	17.4	156.3	1736.1	17361.1
SPOT pan	1	10 × 10	100	0.3	1.0	9.0	100.0	1000.0
SPOT multi	3	20 × 20	400	0.1	0.3	2.3	25.0	250.0
ASTER VNIR	3	15 × 15	225	0.1	0.4	4.0	44.4	444.4
Landsat TM	7	30 × 30	900	0.03	0.1	1.0	11.1	111.1
Landsat ETM+7	7	30 × 30	900	0.03	0.1	1.0	11.1	111.1
Landsat MSS	4	80 × 80	6400	0.004	0.02	0.1	1.6	15.6

2.6.4.2 Multi Source and Multi Temporal Satellite Images

In the last decades, remote sensing has proved a powerful technology for monitoring the earth's surface and atmosphere at a global, regional, and even local scale. This is made possible by the large amount of data acquired by different types of sensors, which provide repeated coverage of the planet on a regular basis. As a consequence, an increasing quantity of multisource and multi temporal remote-sensing data acquired in many geographical areas is available. For a proper exploitation of these data, it is

mandatory to develop effective data fusion techniques able to take advantage of such multisource and multi temporal characteristics. In particular, in the context of classification problems, data fusion may provide an improvement in accuracy (as compared with standard techniques applied to single-sensor/single-date images), which may be of primary importance in real applications.

Data-fusion techniques for the classification of remote sensing images have been extensively investigated in the past years. Many papers that address the development of methodologies for the classification of multi sensor (or multisource) images have been published. Some studies have also been carried out on the integration of the information contained in multi temporal images in order to improve classification accuracy. However, only a few papers have dealt with the integration of both multi sensor and multi temporal remote-sensing images by the data-fusion process (Bungum et al, 2006).